Bioconjugate Chemistry

Article

pubs.acs.org/bc

Self-Assembled Gold Nanoparticle–Fluorescent Protein Conjugates as Platforms for Sensing Thiolate Compounds via Modulation of Energy Transfer Quenching

Anshika Kapur, Fadi Aldeek,[†] Xin Ji,[‡] Malak Safi,[§] Wentao Wang,[‡] Ada Del Cid, Oliver Steinbock, and Hedi Mattoussi*

Department of Chemistry and Biochemistry, Florida State University, Tallahassee, Florida 32306-4390, United States

Supporting Information

ABSTRACT: The ability of Au and other metal nanostructures to strongly quench the fluorescence of proximal fluorophores (dyes and fluorescent proteins) has made AuNP conjugates attractive for use as platforms for sensor development based on energy transfer interactions. In this study, we first characterize the energy transfer quenching of mCherry fluorescent proteins immobilized on AuNPs via metal–histidine coordination, where parameters such as NP size and number of attached proteins are varied. Using steady-state and time-resolved fluorescence measurements, we recorded very high mCherry quenching, with efficiency reaching ~95–97%, independent of the NP size or number of bound fluorophores (i.e., conjugate valence). We further exploited these findings to develop a solution phase sensing platform targeting thiolate compounds. Energy transfer (ET) was employed as a transduction mechanism to monitor the competitive displacement of mCherry from the Au surface upon the introduction of varying amounts of thiolates with different size and coordination numbers. Our results show that the competitive displacement of mCherry depends on the thiolate concentration, time of reaction, and type of thiol derivatives used. Further analysis of the PL recovery data provides a measure for the equilibrium dissociation constant (K_d^{-1}) for these compounds. These findings combined indicate that the AuNP–fluorescent protein conjugates may offer a potentially useful platform for thiol sensing both in solution and in cell cultures.

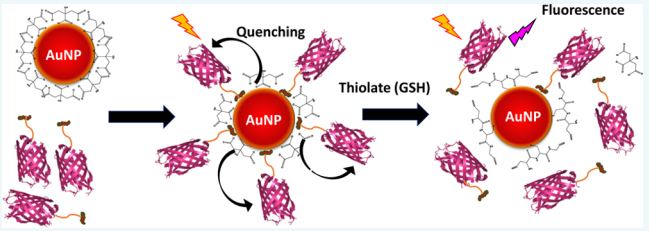

INTRODUCTION

Use of luminescent quantum dots (QDs) and gold nanoparticles (AuNPs) in energy transfer applications has generated a great deal of attention and much activity in the past 2 decades.[1−8] This interest has been motivated by the potential that these materials offer in sensor development both in vitro and in vivo, and by recent advances in engineering a variety of nanoparticles with several unique optical and physical properties.[9−13] QDs have been shown to provide highly effective energy donors when combined with dye and fluorescent protein acceptors, and the interaction mechanism has been largely interpreted within the Förster dipole–dipole interaction model.[2,14−16] Conversely, AuNPs provide strong fluorescence quenchers when paired with dyes as well as QDs, and the extent of energy transfer quenching has been shown to exceed the range stipulated by the Förster process; i.e., the measured quenching efficiency extends over a distance ranging from 1 to 30 nm for metal nanostructures compared to the 1–10 nm range recorded for dye–dye FRET (fluorescence resonance energy transfer). The fluorescence quenching by AuNPs has been discussed within the concepts of nanosurface energy transfer (NSET), involving dipole–surface interactions between the donor fluorophore(s) and the electron-rich surface of the NP.[15,17] Quenching is also affected by the degree of the spectral overlap between the emission of the dye and absorption of the AuNPs.

Due to their nanometer size, these nanocrystals possess large surface-to-volume ratios and they can be coupled to several target molecules such as biomolecules, dyes, and other molecular species. This is beneficial in a variety of biological applications and for implementing energy transfer processes. In particular, it has been shown that a single QD donor can interact simultaneously with several acceptors immobilized on its surface, yielding highly enhanced FRET quenching of QD emission, compared to what is measured for one-donor-to-one-acceptor pair.[14]

Coupling of proteins and peptides appended with a C- or N-terminal polyhistidine sequence to QDs and AuNPs, driven by metal–histidine coordination, has been reported by several groups.[18−20] These interactions require direct access of the imidazoles within the polyhistidine tag to the nanocrystal surfaces. Thus, compact ligands with modest to weak affinity for the metal surface are needed to promote the binding of polyhistidine-appended biomolecules to the nanocrystals.[18,20,21] Furthermore, our group has shown that metal–histidine

Received: January 4, 2017
Published: January 4, 2017

DOI: 10.1021/acs.bioconjchem.7b00006
Bioconjugate Chem. 2017, 28, 678–687

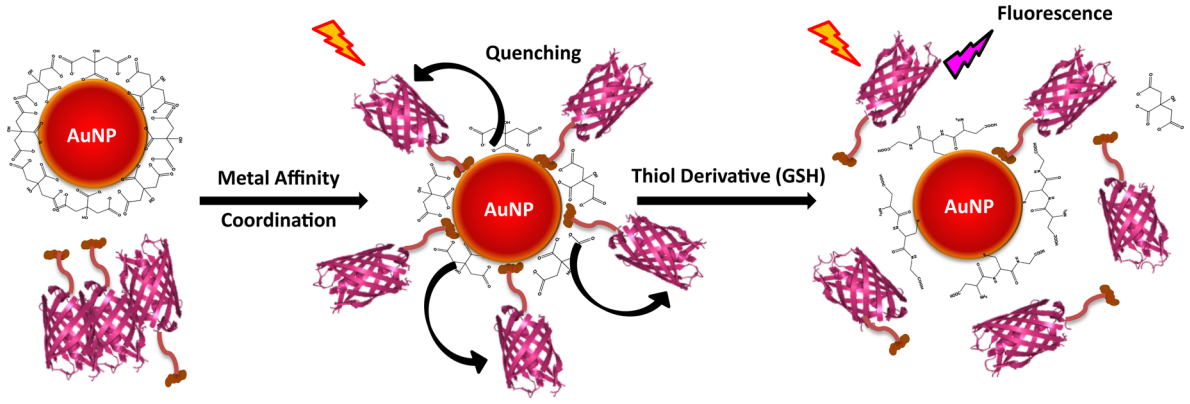

Figure 1. Schematic representation of the conjugation and release strategy. Metal-affinity coordination between citrate AuNPs and histidine tagged mCherry yields AuNP−mCherry conjugates where mCherry fluorescence is quenched. However, addition of thiolate molecules to this medium leads to competitive displacement of mCherry away from the AuNPs and recovery of its fluorescence.

coordination on AuNPs is weaker than that of thiol-appended ligands.[18]

In this study we probe the energy transfer quenching of mCherry fluorescent proteins (mC FPs) self-assembled on citrate-stabilized AuNPs via metal-affinity interactions, where we explore two parameters: (1) the effects of varying the number of proteins per AuNP while maintaining the center-to-center separation distance and (2) the effects of varying the AuNP size; the latter effects permit tuning of the degree of spectral overlap between the emission of the protein donor and the absorbance of the AuNP quencher. In particular, we show that the protein donors interact with the AuNP via individual and independent channels, where each donor experiences the same degree of fluorescence quenching, independent of the total number of proteins per AuNP conjugate. Furthermore, high levels of PL quenching (near unity for the 5 and 13 nm NPs) are measured. This contrasts with findings reported for QD−dye and QD−FP pairs, where each QD simultaneously interacts with each acceptor, and the measured fluorescence quenching results from cumulative interactions with the proximal acceptors (i.e., dyes or fluorescent proteins). Additionally, quenching efficiency rarely reaches unity for those systems.

We then detail the use of these AuNP−mC (or any AuNP−FP) conjugates to probe the competitive displacement of the proteins away from the NP surface by thiolate compounds (RS), using end point fluorescence recovery measurements. This sensor design carefully exploits the fact that imidazole coordination onto Au surfaces is weaker than that of thiolate anchors.[18] More precisely, we probe the effects of introducing different concentrations of small molecule thiolates as well as multidentate thiolate monomers and polymers on the PL recovery. These include the amino acid cysteine, glutathione (a tripeptide), along with several derivatives of lipoic acid (LA in its oxidized form), derivatives of dihydrolipoic acid (the chemically reduced form using $NaBH_4$), and derivatives of the photochemically reduced lipoic acid (*LA-R, using UV irradiation at 350 nm).[22] Estimates of the apparent dissociation constant, $1/K_D$ (with K_D being the binding constant) are extracted from end point PL changes.[18,23] These values are compared (for certain thiolates) to estimates of K_D^{-1} extracted from the on and off rates, k_{on} and k_{off}, for some thiolates (using $K_D^{-1} = k_{off}/k_{on}$). These constants are derived from measurements tracking the time-dependent PL recovery after mixing the conjugates with the competing thiolate molecules.

RESULTS AND DISCUSSION

Assessing the Energy Transfer Quenching in Self-Assembled AuNP−mCherry Conjugates. The mCherry proteins were self-assembled onto citrate-stabilized AuNPs via coordination between the polyhistidine tag on the protein and the metal-rich surfaces of the NPs. This metal coordination driven self-assembly can be applied to AuNPs that either have partially exposed surfaces or are capped with weakly binding ligands such as citrate molecules (see schematics in Figure 1).[18,24,25] This mode of coupling allows for controlled immobilization of proteins on the NP surface, where both the overall orientation and separation distance (from the center of the NP) are preserved for all proteins in the conjugates.[18,26,27] Dispersions of AuNP bioconjugates with varying valences (in a total volume of 500 μL of phosphate buffer) were prepared by mixing aliquots of a stock dispersion of citrate−AuNPs with different volumes of mCherry (stock) solution. Volumes were adjusted to reach AuNP/mCherry molar ratios ranging from 1:0 to 1:12 for 5 nm AuNP and from 1:0 to 1:35 for 13 nm AuNPs; the final NP concentration was fixed at 20 nM and 10 nM for 5 and 13 nm AuNPs, respectively. We used these conjugates as a model system to probe the energy transfer interactions between fluorophores (e.g., fluorescent proteins) and AuNPs. Figure 2A shows representative composite absorption spectra collected from the 5 nm AuNP conjugates. Figure 2B and Figure 2C respectively show the steady-state PL spectra collected from the AuNP−mCherry conjugates and from mCherry solutions (i.e., in the absence of AuNPs). All the samples were excited at 550 nm (near the peak absorption of the protein). It is not possible to prove that conjugation has taken place simply from the absorption spectra shown in Figure 2A, given the extremely weak contribution of the protein to the measured absorbance (ε_{520} (5 nm) = 1.10×10^7 M^{-1} cm^{-1} and ε_{520} (13 nm) = 1.01×10^8 M^{-1} cm^{-1} while ε_{587} (mCherry) = 72 000 M^{-1} cm^{-1}). However, a comparison of the spectra shown in panels B and C indicates that there is a strong quenching of the mCherry emission following conjugation to the AuNPs. Control measurements using mCherry mixed with AuNPs fully passivated with DHLA-PEG-OCH_3 ligands (where no conjugation takes place) show much smaller PL losses (see

DOI: 10.1021/acs.bioconjchem.7b00006
Bioconjugate Chem. 2017, 28, 678−687

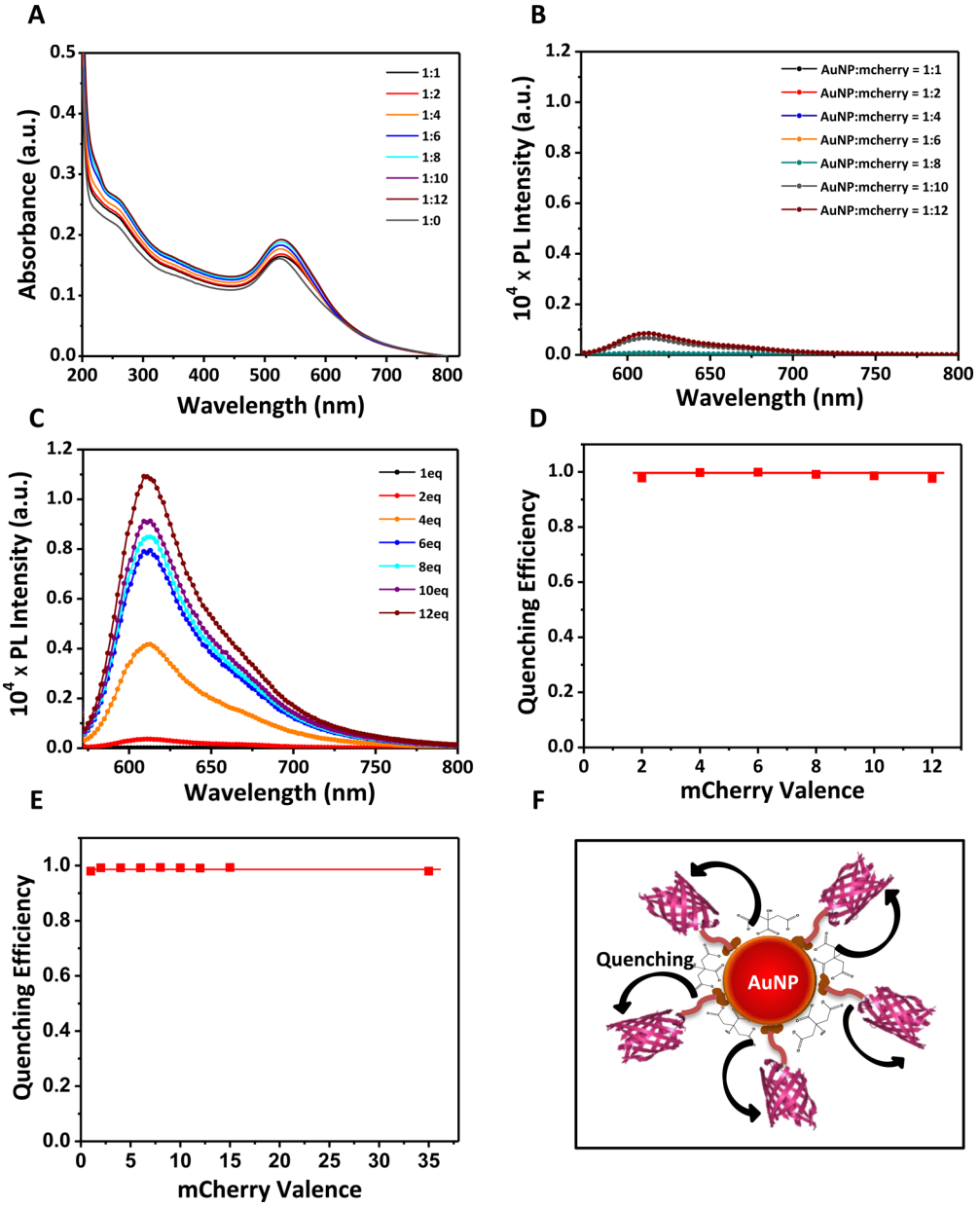

Figure 2. (A) Absorbance spectra collected from AuNP−mCherry conjugates with varying protein-to-NP molar ratios; 5 nm citrate capped AuNPs at concentration of 20 nM were used. (B) Plot shows the PL spectra form the same dispersions in (A). (C) Control experiments showing the PL spectra from mCherry solutions (without AuNPs). (D, E) Plots of the quenching efficiency versus the mCherry-to-AuNP molar ratio for citrate-capped 5 nm (D) and 13 nm (E) AuNPs. (F) Schematic representation of AuNPs interacting individually with each mCherry protein in the quenching process.

Supporting Information, Figure S3).[18] The PL spectra were used to extract values for the quenching efficiencies (E) for dispersions with increasing conjugate valence using the expression[28]

$$E = 1 - \frac{F_{DA}}{F_D} \quad (1)$$

where F_{DA} designates the PL intensity measured from dispersions of mCherry coupled to the AuNPs and F_D is the PL measured from samples made of mCherry alone at the equivalent concentrations. The data in Figure 2D and Figure 2E show that high quenching efficiencies ($E \approx 95-97\%$) are measured for all conditions tested, regardless of the size of the NPs used and essentially independent of the conjugate valence.

The steady-state data are complemented with time-resolved PL measurements, where a significant decrease in the excited-state lifetime of mCherry upon conjugation to the AuNPs is measured for dispersions of AuNP−mCherry conjugates (see Supporting Information, Figure S4). These results are attributed to nonradiative energy transfer quenching of mCherry PL by the central AuNP within each conjugate. This pronounced quenching is promoted by binding of the protein to the AuNP, which brings the mCherry fluorophore in close proximity to the metal surface of the NP.[18] In comparison, the smaller quenching efficiencies measured for the control dispersions (nonconjugated AuNPs and mCherry) result from weaker interactions in the absence of proximity

DOI: 10.1021/acs.bioconjchem.7b00006
Bioconjugate Chem. 2017, 28, 678−687

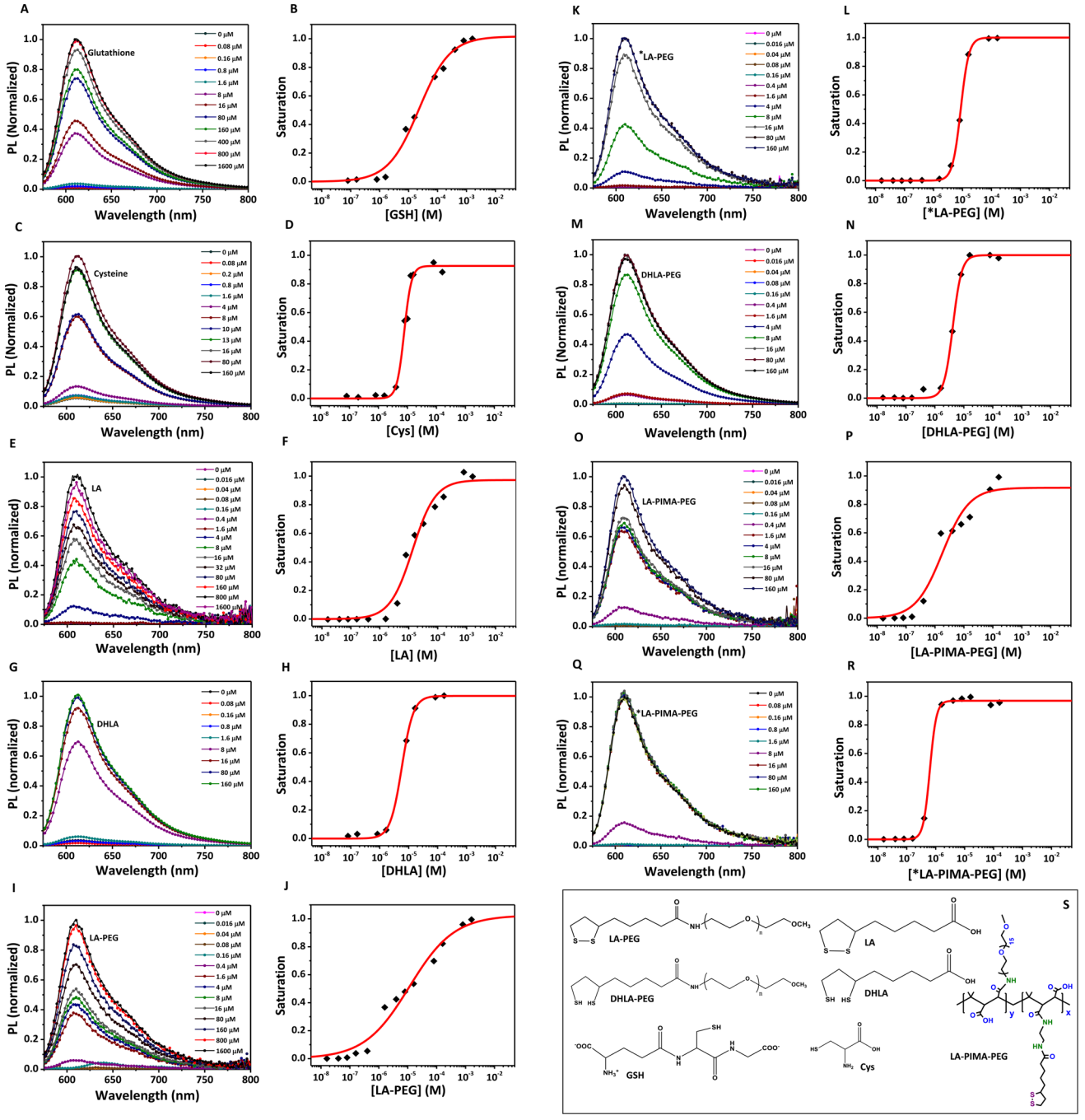

Figure 3. Effect of thiolate addition on the fluorescence properties of AuNP−mCherry conjugates. Shown are the emission spectra along with the saturation curves in response to introducing increasing concentrations of GSH (A, B), cysteine (C, D), LA (E, F), DHLA (G, H), LA−PEG (I, J), *LA−PEG (K, L), DHLA−PEG (M, N) LA−PIMA−PEG (O, P), and *LA−PIMA−PEG (Q, R) with the conjugates. The sign "*" refers to the photochemically reduced ligands. (S) Chemical structures of the various thiolate compounds used in the study.

binding, where energy transfer quenching is primarily due to collisional quenching, characteristic of solution phase samples.

The trend shown in the plot of E vs n for both sets of NPs indicates that the rate of energy transfer quenching is identical for all the FPs within the same conjugate. It reflects that each protein in the assembly interacts with the central AuNP individually and independently of all the other proteins (as schematically depicted in Figure 2F). It further reflects that each protein is positioned at the same average separation distance from the AuNP surface. This behavior is very different from what was reported for QD energy donors surrounded by multiple quenchers (either emitting dyes or redox complexes). In those systems the measured PL quenching efficiency always reflected cumulative interactions of one donor with multiple acceptors.[14] In the present configuration, the plasmonic AuNPs act as an ET "sink" for the excitation of the surrounding fluorophores. To put the above data within a context, we compare the measured quenching efficiencies to theoretical estimates using the Förster model (an approximation) and the dimensions of the AuNP−mCherry assembly. Using an extinction coefficient $\varepsilon_A \cong 1.1 \times 10^7\ M^{-1}\ cm^{-1}$ for the 5 nm NPs and a quantum yield of 0.22 for the mCherry, we estimate

DOI: 10.1021/acs.bioconjchem.7b00006
Bioconjugate Chem. 2017, 28, 678−687

that the Förster distance is ∼10 nm for this pair. Additionally, using the radius of the AuNPs under study and dimensions of the β barrel structure of the protein (5.5 nm × 2.5 nm) and assuming a configuration depicted in Figure 1, we estimate that the center-to-center separation distance including the amino acid linker to be ∼5.5−6 nm for the 5 nm AuNP−mCherry conjugates. Using these values, we estimate a quenching efficiencies E of ∼0.95−0.97, which is rather close to the experimental values measured experimentally. Additional details on the overlap integral and estimate of the Förster radius (R_0) are provided in the Supporting Information.

AuNP−mCherry Conjugates as Platforms for Sensing Thiolate Compounds. The above self-assembled AuNP−mCherry conjugates provide an ideal platform for in vitro and potentially in vivo sensing of molecules that can competitively displace prebound proteins from the NP surface, e.g., competition by added thiolate compounds. This can be quantified by tracking changes in the ET-induced quenching after mixing the conjugates with increasing concentrations of the target molecules. We implemented this approach by investigating the rate of competitive displacement of mCherry from the AuNP surfaces by several soluble thiolate complexes, namely, glutathione, cysteine, and several derivatives of lipoic acid, as a model system; high affinity coordination of thiol groups to Au surfaces has been documented in the literature.[29,30] We explored three aspects: (1) the effects of varying the concentration of solubilized thiolate compounds, (2) their coordination number, and (3) the influence of varying the incubation time on mCherry fluorescence recovery.

In the first set of measurements we collected end point ensemble PL recovery from dispersions of preassembled conjugates that had been mixed with the various thiolates. For this, aliquots from a stock dispersion of AuNP−mCherry conjugates (200 μL, 50 nM, valence of 6) were incubated at room temperature with varying amounts of thiolates in 10 mM phosphate buffer (pH 8) for a period of 1 h. The final concentration of the NP conjugates in each sample was 20 nM in a total volume of 500 μL, while that of thiolates ranged from 0.016 μM to 1600 μM (1.60 mM). A strong recovery in mCherry fluorescence intensity that was commensurate with the concentration of added thiolates was measured (see Figure 3). Control experiments where the thiolates were added to solutions of mCherry yielded no change in the collected fluorescence, confirming that the FP emission is not altered in the presence of these RS molecules (data not shown).

Plots of the relative fluorescence recovery (saturation curves) were generated from the above PL spectra (shown in Figure 3, panels A, C, E, G, I, K, M, O, Q) for all tested compounds using the expression

$$\text{Sat.} = \frac{\text{PL}_{[\text{RS}]} - \text{PL}_{[\text{RS}]=0}}{\text{PL}_{\text{max}}} \tag{2}$$

where $\text{PL}_{[\text{RS}]=0}$ and $\text{PL}_{[\text{RS}]}$ are respectively the integrated PL intensities collected from the conjugate dispersions prior to and after addition of the thiolate at a given concentration, [RS], while PL_{max} is the maximum PL intensity reached at equilibrium. This provided the set of saturation curves shown in Figure 3 (panels B, D, F, H, J, L, N, P, R). We should note that the PL intensities measured at saturation are comparable to those collected from control dispersions of nonconjugated AuNPs and mCherry at the same concentration, which implies that the competitive dissociation of the NP−protein conjugates is essentially complete at high [RS] values (∼0.1−1 mM). The saturation curves can be easily fit to a Hill function of the form

$$y = a\frac{[\text{RS}]^n}{K_\text{d}^{-1} + [\text{RS}]^n} \tag{3}$$

where a is an experimental constant. The best fits to the experimental data were achieved using a variable n (see Figure 3). The value corresponding to 50% saturation provides an estimate for the apparent equilibrium dissociation constant, K_d^{-1}, which essentially accounts for the competitive affinity of the various RS molecules to the AuNPs decorated with several His_6-appended mCherry. We note that the experimental saturation data for the LA derivatives could reasonably be fit to the Hill equation with $n \approx 1$, which is indicative of noncooperative competitive binding of these thiolates to the preassembled conjugates. In comparison, data were better fit with higher order Hill coefficient for derivatives of DHLA and *LA, which suggests that for these thiolate-rich compounds cooperative binding governs the interactions with the conjugates. Conversely, the saturation plots for Cys and GSH are fit to $n > 1$ and $n = 1$, respectively. This may be attributed to the much smaller size of the cysteine and the better exposed thiol group compared to GSH, making its access to the AuNP surface easier. Overall the data indicate that factors such as size of the thiolate molecule, coordination number (monodentate vs bidentate), and solubility in the buffer affect the measured values of K_d^{-1}; higher coordination and better solubility yield lower dissociation constant. For instance, bidentate compounds yield lower K_d^{-1} than monodentate counterparts, attributable to the higher competitive affinity of two thiols vs one thiol to the AuNP surfaces. Conversely, the smaller size Cys exhibited stronger competitive binding than the larger size GSH, which can be correlated to the ability of the small size molecules to better access the areas where the histidine tag coordinates onto the AuNPs. Nonetheless, affinity of the compound to water may play a slight role. DHLA is smaller than DHLA−PEG; however, the latter has slightly higher affinity to water. Both compounds exhibit comparable K_D^{-1} values. The chemically reduced forms of lipoic acid (DHLA) and its derivatives (DHLA−PEG) also show a stronger binding to the AuNP than the oxidized (LA−PEG) or photoreduced (*LA−PEG) counterparts. Similarly, higher K_d^{-1} was measured for the oxidized polymer (LA−PIMA−PEG) than for the photochemically modified counterpart (*LA−PIMA−PEG). These results are consistent with previous data collected using the Ellman assay, where we found that the concentration of dithiol groups is lowest in LA derivatives (negligible amounts) but reaches ∼40−60% of the total thiolates in solutions of photoirradiated compounds and 95−99% of the total thiolates for solutions of chemically reduced DHLA derivatives.[22]

It would be highly informative to complement the above data with additional information about the kinetics of competitive binding of thiolates to the AuNPs. The kinetics for such systems with multicoordinating protein and the large surface area presented on a NP are very complex, nonetheless. To develop some insights into this issue, we proceeded to monitor the kinetics of mCherry fluorescence recovery immediately following the addition of the thiolate molecules to the AuNP−mCherry conjugate dispersions. For this, a solution of mCherry (in buffer) was first loaded into a cuvette and a series of 2 s signal acquisitions at the mCherry emission peak (610 nm) were collected using excitation at 550 nm, until the intensity

DOI: 10.1021/acs.bioconjchem.7b00006
Bioconjugate Chem. 2017, 28, 678−687

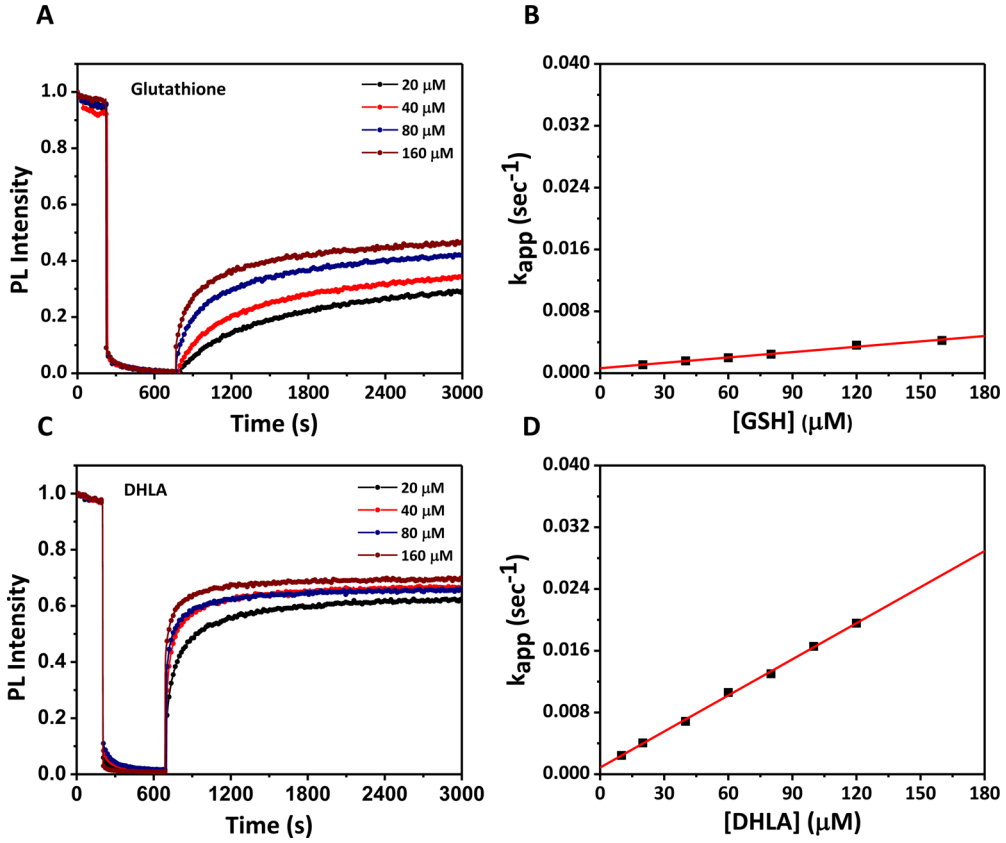

Figure 4. Representative time traces showing the mCherry PL of protein alone, PL of mCherry following their self-assembly with the AuNPs (t = 250 s), and PL recovery after mixing the conjugates with the respective concentrations of GSH (A) and DHLA (C) (t = 750 s). Plot of the apparent binding rates k_{app} vs thiol concentration, together with the corresponding k_{on} and k_{off} rates for GSH (B) and DHLA (D).

was stabilized. Then, an aliquot of AuNP dispersion was added to a final protein/AuNP molar ratio of 6:1. Immediate drop in the PL was recorded, due to rapid conjugate formation, followed by saturation at near zero intensity after ∼10−15 min. This corresponds to equilibrium where all added mCherry proteins are essentially self-assembled onto the AuNPs. Once equilibrium was reached, an aliquot of RS solution was rapidly mixed into the dispersion and the fluorescence signal acquisition was resumed until the intensity reached a plateau (usually after 20−30 min), corresponding to equilibrium between bound and free mCherry in the medium following competitive displacement away from the NP surfaces initiated by the RS thiolates. The experiment was repeated for several concentrations and further applied to two thiolate compounds used (GSH and DHLA). Two representative time-dependent PL intensity profiles collected at several [RS] values are shown in Figure 4A,C. Note that the data shown in Figure 4 contain kinetic data on the self-assembly of mCherry onto the AuNPs reflected by the fast decay of the FP PL following the addition of AuNPs to the mCherry solution. They are also very informative for extracting information on the polyimidazole-driven AuNP−mC conjugate formation. We have indeed carried out a thorough analysis of the AuNP−mC self-assembly and extracted values for the association and dissociation rates along with a value for the dissociation constant, as detailed in our previous publication.[18]

The PL recovery curves for GSH exhibit a fast initial rise in mCherry emission, followed by slower increase until saturation is reached at longer time. Such recovery is substantially faster for DHLA, with most of the PL increase occurring between the introduction of the thiolate and resumption of the signal collection. The PL recovery collected after mixing the conjugates with other thiolates is even faster (data not shown). The signal recovery is essentially too fast to resolve with this experimental procedure. Analysis of the kinetics of the thiolate binding using the PL recovery data is rather challenging and involves a more intricate mechanism. Indeed, the release of one mCherry likely requires the competitive coordination of a few thiolates (∼1−6, given that each protein is coordinated on the NP via a 6-histidine tail). We are presently exploring theoretical models to account for the fast kinetics and their dependence on parameters such as thiolate coordination number, size, and concentration.

Nonetheless, we have attempted to extract some useful information on the AuNP−mCherry−plus-GSH and AuNP−mCherry−plus-DHLA systems. The slower PL recovery in the presence of these thiolates may be treated within the framework of a pseudo first order bimolecular interactions model, which is a phenomenological approach. We can reasonably assume that release events of distinct mCherry proteins, either from the same NP or from different NPs, are independent. In addition, because the citrate coordination on the AuNPs is overall weak compared to the binding of both His-protein and thiolates, we can ignore the competition of those native ligands with the added thiolates for coordination on the nanocrystal surfaces. Within these approximations and using the above experimental conditions, the relative PL recovery upon mCherry protein release at a given time (t) will depend on the concentration of bound thiolates, [RS](t), which can be expressed in terms of

DOI: 10.1021/acs.bioconjchem.7b00006
Bioconjugate Chem. 2017, 28, 678−687

Table 1. Comparison of K_d^{-1} Values Obtained for GSH, Cys, LA, DHLA, and PEG derivatives of LA, DHLA, and *LA Using End-Point Fluorescence, along with Values of k_{on}, k_{off}, and K_d^{-1} Obtained from Time-Dependent Fluorescence Recovery Analyses Limited to GSH and DHLA

		kinetics of PL recovery			
RS compd	end point PL recovery, K_d^{-1} (μM)	k_{on} (μM^{-1} s^{-1})	k_{off} (s^{-1})	K_d^{-1} (μM)	n
GSH	22.9 ± 4.5	0.23	6.46	28	0.8 ± 0.09
Cys	7.7 ± 0.43				3.4 ± 0.6
LA	13.6 ± 2.2				1.1 ± 0.17
DHLA	5.8 ± 0.3	1.56	8.63	5.53	2.2 ± 0.2
LA–PEG_{750}	11.3 ± 4.4				0.56 ± 0.09
LA–PEG_{750}[a]	8.7 ± 0.12				3 ± 0.1
DHLA–PEG_{750}	4.2 ± 0.13				2.8 ± 0.25
LA–PIMA–PEG_{750}	1.8 ± 0.62				0.9 ± 0.2
LA–PIMA–PEG_{750}[a]	0.63 ± 0.036				3.8 ± 0.5

[a]Represents the photochemically reduced ligands.

the initial thiolate concentration at $t = 0$ ($[RS]_0$) and the apparent binding constant, k_{app}, as shown in eq 3:[23]

$$[mC](t) \propto [RS](t) = [RS]_0(1 - e^{-k_{app}t}) \quad (4)$$

Within this analysis, the time-dependent PL recovery of mCherry, $PL_{mC}(t)$, can be fit to an expression of the form

$$PL_{mC}(t) = PL_0 + \Delta PL(1 - e^{-k_{app}t}) \quad (5)$$

where PL_0 designates the fluorescence intensity measured at $t = 0$ (i.e., prior to the addition of the RS compound) and ΔPL corresponds to the total difference between the mCherry PL measured at saturation (asymptotic limit reached at equilibrium) and PL_0.

The changes in mCherry signal after addition of RS (shown in Figure 4A,C) were fit to eq 5, yielding a measure for k_{app} at several concentrations for each compound. Furthermore, fitting the k_{app} values to a linear function of the form

$$k_{app} = k_{on}[RS]_0 + k_{off} \quad (6)$$

allowed us to derive values for k_{on} (from the slope) and k_{off} (from the intercept at $[RS]_0 = 0$), which are respectively associated with the competitive binding and unbinding of the thiolates to the AuNPs (in the presence of mCherry), as illustrated in the panels shown in Figure 4B,D. From the above values for k_{on} and k_{off}, one can extract a value for the dissociation constant defined as

$$K_d^{-1} = \frac{k_{off}}{k_{on}} \quad (7)$$

The values for K_d^{-1} extracted for GSH and DHLA are close to those extracted from the saturation data; see Table 1. We are presently exploring a few theoretical concepts to describe the competitive interaction of the thiol groups with varying coordination, size, and solubility on the PL recovery of the mCherry. We are exploring the effects of changing the conjugate valence as well as the nature of the metal NP used. Results from those findings will be discussed in future works.

To test the specificity of thiolate competition for the AuNP surface with the preassembled AuNP–mCherry conjugate, we tentatively tested the effects of introducing small molecule analytes such as imidazole and the amino acid aspartic acid on the overall measured PL. For this, AuNP–mCherry conjugates (prepared with a molar ratio of AuNP/mCherry =1:10) were incubated with increasing concentrations of aspartic acid or imidazole for 2 h, after which the PL spectra were collected. We also tested the colloidal stability and integrity of the conjugate assemblies in the presence of 10% serum in buffer and in media mimicking physiological conditions. Conjugates with high valence were used to avoid potential interference from electrostatic interactions between the remaining surface-coordinated citrates with amino acid. We measured a PL quenching of mCherry of ~95–96% in all cases. This clearly proves that no release of mCherry from the nanoparticle surface has taken place even in serum rich media or in the presence of excess aspartic acid or imidazole (see Figure 5).

These results combined imply that the AuNP–mC (or in general any AuNP–FP) conjugates offer a promising platform for sensing the presence and competitive coordination of thiolates species in vitro and potentially inside live cells. Furthermore, given the rather large difference between the affinities of thiolate vs imidazole to gold, conjugates made of AuNPs decorated with various His-appended biomolecules could provide great platforms for targeted intracellular delivery of cargo proteins and nucleic acids, where the native intracellular thiols could promote the release of biomolecules or therapeutic drugs preassembled onto the AuNPs. Additionally, the competitive disassembly/dissociation of the AuNP–FP conjugates, driven by the added thiolates, produces a net turn on PL signal (from the nearly 100% quenched emission). This bodes well for in vivo sensing where background contribution is reduced.

CONCLUSION

In this report, we characterized the quenching of mCherry fluorescence by AuNPs promoted by energy transfer interactions in AuNP–mCherry conjugates, assembled via metal-affinity coordination between the imidazole groups in the protein and the gold surfaces. Steady-state fluorescence measurements indicated that the energy transfer quenching for these assemblies reached near unity for 5 and 13 nm NPs. Additionally, the proteins interact with the central AuNP via independent energy transfer channels, where the NP acts as an energy sink for the protein excitation.

We then demonstrated the potential use of these assemblies in sensing applications, in particular, solution phase sensing of thiolate compounds, including GSH, Cys, LA, and LA derivatives. The thiolate groups competitively displace the mCherry from the AuNPs, resulting in progressive PL recovery. This competitive displacement was found to depend on the thiol concentration, time of reaction, and type of thiol derivatives used. We extracted estimates for the association

DOI: 10.1021/acs.bioconjchem.7b00006
Bioconjugate Chem. 2017, 28, 678–687

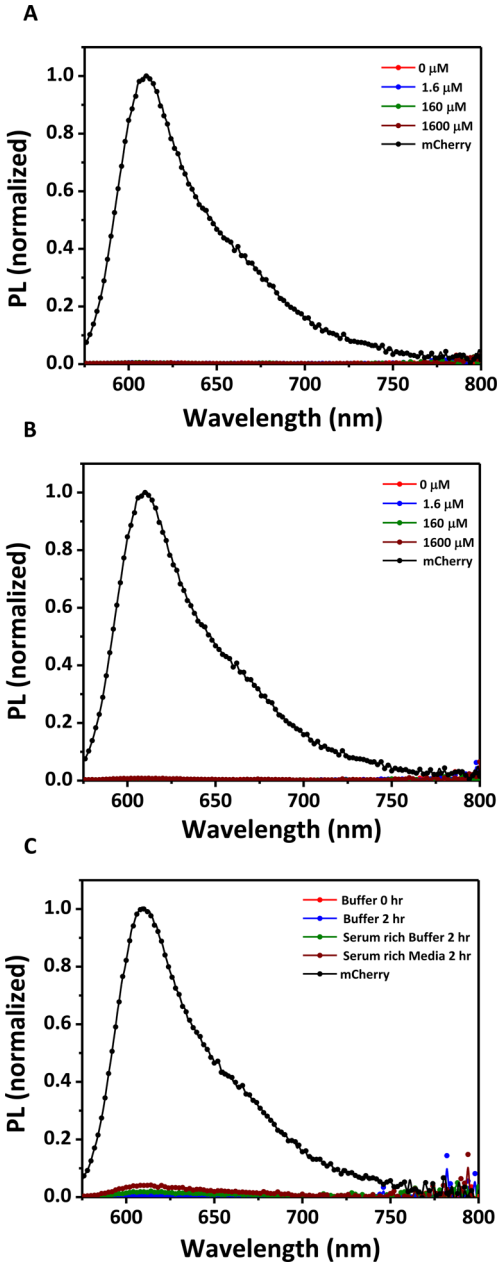

Figure 5. Testing the specificity of the AuNP−mCherry platforms toward thiolate analytes. Shown are the photoluminescence spectra of AuNP−mCherry conjugate dispersions in the presence of increasing concentrations of aspartic acid (A) and imidazole (B). Spectra were collected 1 h after mixing and incubation. Also shown are the PL spectra of AuNP−mCherry conjugate dispersions in pure buffer, buffer mixed with 10% fetal bovine serum, and DMEM media supplemented with 10% fetal bovine serum collected 2 h after mixing (C).

and dissociation rates along with the equilibrium dissociation constant for two representative thiolates. We found that differences in K_d^{-1} are governed by the number and availability of thiol groups in the RS molecule used. Higher thiol coordination and smaller size compounds yielded smaller dissociation constants.

It would be interesting to further explore, in future works, the effects of additional variables in the system, including the starting AuNP−FP conjugate valence and different thiolate compounds (e.g., multidentate oligomers). Biothiols are known to play crucial roles in several biological processes, and the levels of thiol containing substances in biological systems have been correlated with different diseases.[31−34] Hence, the desire to develop quantitative assessment of these substances has gathered much attention in the past decade.[35,36] Furthermore, the presence of abundant amounts of thiol compounds inside cells has been investigated in cellular delivery studies.[37,38] Our results indicate that this sensing configuration can be generalized to an array of other thiolate compounds. Indeed, intracellular GSH-triggered release of biomolecules coupled to AuNPs has been investigated as a means of delivering target biomolecules inside live cells.[37−39] In this context our system provides a promising platform for delivering biomolecules/drugs inside cells by combining the metal−histidine coordination and competitive thiol-triggered release of immobilized target molecules from the AuNPs.

EXPERIMENTAL SECTION

Reagents. Tetrachloroauric(III) acid trihydrate ($HAuCl_4 \cdot 3H_2O$) (99.9%), (±-α-lipoic acid) (LA), poly(ethylene glycol) methyl ether ($M_w \approx 750$), sodium borohydride ($NaBH_4$), sodium citrate tribasic dihydrate ($C_6H_5Na_3O_7 \cdot 2H_2O$), L-glutathione reduced, and cysteine were purchased from Sigma Chemicals (St. Louis, MO). L-Aspartic acid was purchased from VWR AMRESCO Life Sciences (Solon, OH), and imidazole was purchased from Scharlab (Barcelona, Spain).

Growth of Citrate-Stabilized AuNPs. The 5 nm citrate-stabilized AuNPs used in this study were grown following literature protocols.[18] Briefly, 250 μL of 50 mM aqueous solution of $HAuCl_4 \cdot 3H_2O$ was mixed with 50 mL of water, and the mixture was stirred for approximately 1 min. Then, 1 mL of a 38.8 mM aqueous solution of sodium citrate was added. In a separate vial, 100 μL of 200 mM $NaBH_4$ was mixed with 900 μL of 38.8 mM sodium citrate solution. This content was rapidly injected in the above flask (containing the $HAuCl_4$ solution), and the mixture was stirred for 2 h, followed by purification of the nanoparticles by applying one cycle of centrifugation/filtration using a membrane filtration device (Millipore) with a cutoff molecular weight of 50 kDa.

The 13 nm diameter citrate-stabilized AuNPs were grown following a procedure reported by Turkevich.[40] Briefly, an amount of 50 mL of 1 mM $HAuCl_4 \cdot 3H_2O$ aqueous solution was added to 100 mL Erlenmeyer flask equipped with a magnetic stirring bar. This solution was heated to 100 °C and 50 mg of sodium citrate tribasic dihydrate dissolved in 2 mL of DI water was added. The stirring was continued for an additional 15 min, and heating was stopped when a deep red color was obtained. The solution was then purified by applying one cycle of centrifugation/filtration using a membrane filtration device (Millipore) with a molecular weight cutoff of 50 kDa.

AuNP−mCherry−His Conjugate Preparation. Dispersions of AuNP−mCherry−His_6 conjugates in PBS buffer with a wide range of valences were prepared and tested. Conjugate preparation was carried out by mixing, in an Eppendorf tube, aliquots of AuNP dispersions and mCherry solutions starting with stock samples of given molar concentrations in phosphate buffer (10 mM, pH 8) and left to incubate for 1 h at 4 °C; a total of 500 μL was used for each sample. The molar concentration of mCherry was determined using its extinction coefficient $\varepsilon_{587} = 72\,000\ M^{-1}\ cm^{-1}$, while those of AuNPs were determined using the extinction coefficients of ε_{520}(5 nm) = $1.10 \times 10^7\ M^{-1}\ cm^{-1}$ and ε_{520}(13 nm) = $1.01 \times 10^8\ M^{-1}\ cm^{-1}$ (Sigma-Aldrich).[41] In a typical preparation of 5 nm AuNP

DOI: 10.1021/acs.bioconjchem.7b00006
Bioconjugate Chem. 2017, 28, 678−687

conjugates, fixed volume aliquots of a stock dispersion of citrate−AuNPs were mixed with different volumes of mCherry (stock) solution, where the final molar ratio of AuNP:mCherry in each sample was varied from 1:0 to 1:12; the AuNP concentration was fixed at 20 nM. Anticipating a complete association between the NP and protein, driven by metal−histidine coordination, this would yield dispersions of AuNP−mCherry conjugates with an average valence ranging from 1 to 12.[18] A similar protocol was applied to conjugate the His-tagged mCherry onto the 13 nm AuNPs except that the protein-to-AuNP molar ratio was varied between 0:1 and 35:1. Following self-assembly the samples were characterized using UV−vis absorption spectroscopy. Inspecting the absorption of the various mixtures provided a first test of the conjugate formation and allowed us to verify that the integrity of the AuNPs and mCherry proteins was maintained following self-assembly. The absorption data were complemented with steady-state fluorescence measurements, which ultimately proved close proximity between the protein and the NP (i.e., binding) and yielded information about the nature of energy transfer interactions in these assemblies.

Competitive Displacement of mCherry and Fluorescence Recovery Assay. The competitive displacement of the mCherry away from the AuNP surfaces by RS molecules was tested using several compounds, namely, GSH, cysteine, LA, DHLA, LA appended with a polyethylene glycol short chain (LA−PEG_{750}), DHLA−PEG_{750}, LA−PIMA−PEG_{750} (a polymer), *LA−PEG_{750}, *LA−PIMA−PEG_{750}. Dispersions of AuNP−mCherry conjugates with an average valence of 6 and at a NP concentration of 50 nM were assembled and left to equilibrate for 1 h, yielding highly quenched samples. To each dispersion, aliquots of a given RS compound (from a stock solution) dissolved in PB buffer (10 mM, pH 8) were added. The prepared solutions were diluted with buffer to 500 μL, and the AuNP concentration was maintained at 20 nM for all measurements. Competitive displacement of the protein from the NP surfaces was assessed by analyzing the end point PL changes (compared to the initial values) for several concentrations of the thiolate compounds. In addition, we analyzed the time-dependent PL recovery for several concentrations of two compounds, GSH and DHLA. This has allowed us to compare the information extracted from both analyses, at least for two simple thiolates.

Instrumentation. The optical absorption spectra were collected using a Shimadzu UV−vis absorption spectrophotometer (UV 2450 model from Shimadzu). The PL spectra were collected using either a fluorescence array reader (Infinite M1000Tecan plate reader, TECAN, Research Triangle Park, NC) or a Fluorolog-3 spectrometer (HORIBA Jobin Yvon Inc., Edison, NJ) equipped with a PMT detector. The fluorescence lifetime measurements were collected on a time correlation single photon counting (TCSPC) system integrated into the same Fluorolog-3, where a pulsed excitation signal at 440 nm with a repetition rate of 1 MHz provided by NanoLED-440LH (100 ps, fwhm) was used. The time progression of the PL recovery profiles was also collected using the Fluorolog-3 spectrometer.

■ ASSOCIATED CONTENT

Supporting Information

The Supporting Information is available free of charge on the ACS Publications website at DOI: 10.1021/acs.bioconjchem.7b00006.

Additional information and data on the mCherry expression, ligand synthesis, photochemical modification, energy transfer analysis, absorption and emission spectra from self-assembly prepared using 13 nm AuNPs, PL spectra from control samples with 5 nm AuNPs, and time-resolved fluorescence profiles (PDF)

■ AUTHOR INFORMATION

Corresponding Author

*E-mail: mattoussi@chem.fsu.edu.

ORCID

Hedi Mattoussi: 0000-0002-6511-9323

Present Addresses

[†]F.A.: Florida Department of Agriculture, Division of Food Safety, 3125 Conner Boulevard, Tallahassee, FL 32399.

[‡]X.J. and W.W.: Ocean Nanotech, LLC, 7964 Arjons Drive, San Diego, CA 92126.

[§]M.S.: Laboratoire de Physique des Solides, Université Paris-Sud, 1 Rue Nicolas Appert, 91405 Orsay Cedex, France.

Notes

The authors declare no competing financial interest.

■ ACKNOWLEDGMENTS

We thank the National Science Foundation (NSF-CHE, Grants 1058957 and 1508501). We also thank Goutam Palui and Naiqian Zhan for fruitful discussions.

■ REFERENCES

(1) Saha, K., Agasti, S. S., Kim, C., Li, X. N., and Rotello, V. M. (2012) Gold Nanoparticles in Chemical and Biological Sensing. *Chem. Rev. 112*, 2739−2779.

(2) Medintz, I. L., and Mattoussi, H. (2009) Quantum dot-based resonance energy transfer and its growing application in biology. *Phys. Chem. Chem. Phys. 11*, 17−45.

(3) Li, M., Cushing, S. K., Wang, Q. Y., Shi, X. D., Hornak, L. A., Hong, Z. L., and Wu, N. Q. (2011) Size-Dependent Energy Transfer between CdSe/ZnS Quantum Dots and Gold Nanoparticles. *J. Phys. Chem. Lett. 2*, 2125−2129.

(4) Ji, X., Wang, W., and Mattoussi, H. (2016) Controlling the spectroscopic properties of quantum dots via energy transfer and charge transfer interactions: Concepts and applications. *Nano Today 11*, 98−121.

(5) Freeman, R., and Willner, I. (2012) Optical molecular sensing with semiconductor quantum dots (QDs). *Chem. Soc. Rev. 41*, 4067−4085.

(6) Zhou, J., Yang, Y., and Zhang, C.-y. (2015) Toward Biocompatible Semiconductor Quantum Dots: From Biosynthesis and Bioconjugation to Biomedical Application. *Chem. Rev. 115*, 11669−11717.

(7) Howes, P. D., Chandrawati, R., and Stevens, M. M. (2014) Colloidal nanoparticles as advanced biological sensors, *Science 346*, DOI: 10.1126/science.1247390.

(8) Boles, M. A., Ling, D., Hyeon, T., and Talapin, D. V. (2016) The surface science of nanocrystals. *Nat. Mater. 15*, 141−153.

(9) Delehanty, J. B., Medintz, I. L., Pons, T., Brunel, F. M., Dawson, P. E., and Mattoussi, H. (2006) Self-assembled quantum dot-peptide bioconjugates for selective intracellular delivery. *Bioconjugate Chem. 17*, 920−927.

(10) Faraji, A. H., and Wipf, P. (2009) Nanoparticles in cellular drug delivery. *Bioorg. Med. Chem. 17*, 2950−2962.

(11) Han, G., Ghosh, P., and Rotello, V. (2007) Multi-Functional Gold Nanoparticles for Drug Delivery. In *Bio-Applications of Nanoparticles* (Chan, W. W., Ed.), pp 48−56, Springer, New York.

DOI: 10.1021/acs.bioconjchem.7b00006
Bioconjugate Chem. 2017, 28, 678−687

(12) Farokhzad, O. C., and Langer, R. (2006) Nanomedicine: Developing smarter therapeutic and diagnostic modalities. *Adv. Drug Delivery Rev. 58*, 1456−1459.
(13) Xu, Z. P., Zeng, Q. H., Lu, G. Q., and Yu, A. B. (2006) Inorganic nanoparticles as carriers for efficient cellular delivery. *Chem. Eng. Sci. 61*, 1027−1040.
(14) Clapp, A. R., Medintz, I. L., Mauro, J. M., Fisher, B. R., Bawendi, M. G., and Mattoussi, H. (2004) Fluorescence resonance energy transfer between quantum dot donors and dye-labeled protein acceptors. *J. Am. Chem. Soc. 126*, 301−310.
(15) Pons, T., Medintz, I. L., Sapsford, K. E., Higashiya, S., Grimes, A. F., English, D. S., and Mattoussi, H. (2007) On the quenching of semiconductor quantum dot photoluminescence by proximal gold nanoparticles. *Nano Lett. 7*, 3157−3164.
(16) Singh, M. P., and Strouse, G. F. (2010) Involvement of the LSPR Spectral Overlap for Energy Transfer between a Dye and Au Nanoparticle. *J. Am. Chem. Soc. 132*, 9383−9391.
(17) Jennings, T. L., Singh, M. P., and Strouse, G. F. (2006) Fluorescent lifetime quenching near d = 1.5 nm gold nanoparticles: probing NSET validity. *J. Am. Chem. Soc. 128*, 5462−5467.
(18) Aldeek, F., Safi, M., Zhan, N. Q., Palui, G., and Mattoussi, H. (2013) Understanding the Self-Assembly of Proteins onto Gold Nanoparticles and Quantum Dots Driven by Metal-Histidine Coordination. *ACS Nano 7*, 10197−10210.
(19) Sapsford, K. E., Algar, W. R., Berti, L., Gemmill, K. B., Casey, B. J., Oh, E., Stewart, M. H., and Medintz, I. L. (2013) Functionalizing Nanoparticles with Biological Molecules: Developing Chemistries that Facilitate Nanotechnology. *Chem. Rev. 113*, 1904−2074.
(20) Petryayeva, E., Algar, W. R., and Krull, U. J. (2013) Adapting Fluorescence Resonance Energy Transfer with Quantum Dot Donors for Solid-Phase Hybridization Assays in Microtiter Plate Format. *Langmuir 29*, 977−987.
(21) Mattoussi, H., Mauro, J. M., Goldman, E. R., Anderson, G. P., Sundar, V. C., Mikulec, F. V., and Bawendi, M. G. (2000) Self-assembly of CdSe-ZnS quantum dot bioconjugates using an engineered recombinant protein. *J. Am. Chem. Soc. 122*, 12142−12150.
(22) Aldeek, F., Hawkins, D., Palomo, V., Safi, M., Palui, G., Dawson, P. E., Alabugin, I., and Mattoussi, H. (2015) UV and Sunlight Driven Photoligation of Quantum Dots: Understanding the Photochemical Transformation of the Ligands. *J. Am. Chem. Soc. 137*, 2704−2714.
(23) Sapsford, K. E., Pons, T., Medintz, I. L., Higashiya, S., Brunel, F. M., Dawson, P. E., and Mattoussi, H. (2007) Kinetics of metal-affinity driven self-assembly between proteins or peptides and CdSe-ZnS quantum dots. *J. Phys. Chem. C 111*, 11528−11538.
(24) Kogot, J. M., Parker, A. M., Lee, J., Blaber, M., Strouse, G. F., and Logan, T. M. (2009) Analysis of the Dynamics of Assembly and Structural Impact for a Histidine Tagged FGF1-1.5 nm Au Nanoparticle Bioconjugate. *Bioconjugate Chem. 20*, 2106−2113.
(25) Kogot, J. M., England, H. J., Strouse, G. F., and Logan, T. M. (2008) Single Peptide Assembly onto a 1.5 nm Au Surface via a Histidine Tag. *J. Am. Chem. Soc. 130*, 16156−16157.
(26) Palui, G., Aldeek, F., Wang, W. T., and Mattoussi, H. (2015) Strategies for interfacing inorganic nanocrystals with biological systems based on polymer-coating. *Chem. Soc. Rev. 44*, 193−227.
(27) Medintz, I. L., Konnert, J. H., Clapp, A. R., Stanish, I., Twigg, M. E., Mattoussi, H., Mauro, J. M., and Deschamps, J. R. (2004) A fluorescence resonance energy transfer-derived structure of a quantum dot-protein bioconjugate nanoassembly. *Proc. Natl. Acad. Sci. U. S. A. 101*, 9612−9617.
(28) Lakowicz, J. R. (2006) *Principles of Fluorescence Spectroscopy*, 3rd ed., Springer, New York.
(29) Xue, Y., Li, X., Li, H., and Zhang, W. (2014) Quantifying thiol−gold interactions towards the efficient strength control. *Nat. Commun. 5*, 4348.
(30) Pensa, E., Cortés, E., Corthey, G., Carro, P., Vericat, C., Fonticelli, M. H., Benítez, G., Rubert, A. A., and Salvarezza, R. C. (2012) The Chemistry of the Sulfur−Gold Interface: In Search of a Unified Model. *Acc. Chem. Res. 45*, 1183−1192.
(31) Wood, Z. A., Schröder, E., Robin Harris, J., and Poole, L. B. (2003) Structure, mechanism and regulation of peroxiredoxins. *Trends Biochem. Sci. 28*, 32−40.
(32) White, A. C., Thannickal, V. J., and Fanburg, B. L. (1994) Glutathione deficiency in human disease. *J. Nutr. Biochem. 5*, 218−226.
(33) Seshadri, S., Beiser, A., Selhub, J., Jacques, P. F., Rosenberg, I. H., D'Agostino, R. B., Wilson, P. W., and Wolf, P. A. (2002) Plasma homocysteine as a risk factor for dementia and Alzheimer's disease. *N. Engl. J. Med. 346*, 476−483.
(34) Munday, R. (1989) Toxicity of thiols and disulphides: Involvement of free-radical species. *Free Radical Biol. Med. 7*, 659−673.
(35) Ang, C. Y., Tan, S. Y., Lu, Y., Bai, L., Li, M., Li, P., Zhang, Q., Selvan, S. T., and Zhao, Y. (2014) "Turn-on" fluorescence probe integrated polymer nanoparticles for sensing biological thiol molecules. *Sci. Rep. 4*, 7057.
(36) Gao, Y., Li, Y., Zou, X., Huang, H., and Su, X. (2012) Highly sensitive and selective detection of biothiols using graphene oxide-based "molecular beacon"-like fluorescent probe. *Anal. Chim. Acta 731*, 68−74.
(37) Han, G., Chari, N. S., Verma, A., Hong, R., Martin, C. T., and Rotello, V. M. (2005) Controlled Recovery of the Transcription of Nanoparticle-Bound DNA by Intracellular Concentrations of Glutathione. *Bioconjugate Chem. 16*, 1356−1359.
(38) Hong, R., Han, G., Fernández, J. M., Kim, B.-j., Forbes, N. S., and Rotello, V. M. (2006) Glutathione-Mediated Delivery and Release Using Monolayer Protected Nanoparticle Carriers. *J. Am. Chem. Soc. 128*, 1078−1079.
(39) Wang, X., Cai, X., Hu, J., Shao, N., Wang, F., Zhang, Q., Xiao, J., and Cheng, Y. (2013) Glutathione-Triggered "Off−On" Release of Anticancer Drugs from Dendrimer-Encapsulated Gold Nanoparticles. *J. Am. Chem. Soc. 135*, 9805−9810.
(40) Turkevich, J., Stevenson, P. C., and Hillier, J. (1951) A study of the nucleation and growth processes in the synthesis of colloidal gold. *Discuss. Faraday Soc. 11*, 55−75.
(41) Oh, E., Susumu, K., Goswami, R., and Mattoussi, H. (2010) One-Phase Synthesis of Water-Soluble Gold Nanoparticles with Control over Size and Surface Functionalities. *Langmuir 26*, 7604−7613.

DOI: 10.1021/acs.bioconjchem.7b00006
Bioconjugate Chem. 2017, 28, 678−687